Hindawi
Geofluids
Volume 2024, Article ID 4572483, 9 pages
https://doi.org/10.1155/2024/4572483

Research Article

A Numerical Simulation Approach for Superheated Steam Flow during Multipoint Steam Injection in Horizontal Well

Qiuying Du, Mingzhong Li, Chenwei Liu, Zhifeng Bai, Chenru Zhou, and Xiangyu Wang

School of Petroleum Engineering, China University of Petroleum, Qingdao 266580, China

Correspondence should be addressed to Mingzhong Li; limingzhong_upc@hotmail.com

Received 4 September 2022; Revised 12 October 2022; Accepted 23 January 2023; Published 19 January 2024

Academic Editor: Yiding Bao

Superheated steam flow during multipoint steam injection technology has a good effect on improving the steam absorption profile of heavy oil thermal recovery wells, enhancing the production degree of horizontal section of thermal recovery wells, and enhancing oil recovery. Based on the structure of multipoint steam injection horizontal string, considering the characteristics of variable mass flow, pressure drop of steam-liquid two-phase flow, and throttling pressure difference of steam injection valve in the process of steam injection, this paper establishes the calculation model of various parameters of multipoint steam injection horizontal wellbore and calculates the distribution of steam injection rate, temperature, pressure gradient, and dryness along the section of multipoint steam injection in horizontal wellbore. The results show that the temperature and pressure decrease gradually from heel to toe, and the steam dryness decreases gradually. Considering the influence of throttle pressure difference of steam injection valve and pressure drop of gas-liquid two-phase flow in the wellbore, the traditional calculation model of steam injection thermodynamic parameters is optimized, and the optimization of wellbore structure and steam injection parameters is an effective method to achieve uniform steam injection in horizontal wells. The steam injection uniformity of horizontal wells can be effectively improved by adjusting the steam injection valve spacing and steam injection parameters. When the steam injection volume is 200 m^3/d and the steam injection valve spacing is 20 m, a more stable steam injection effect can be obtained. The findings of this study can help for better understanding of improving the uniformity of steam injection and enhancing the recovery factor.

1. Introduction

In the process of heavy oil production, the horizontal well has a large contact area with the reservoir, the range of steam injection is wide, and the productivity is higher than that of the vertical well [1, 2]. The multipoint steam injection technology in horizontal wells is widely used to improve the uniformity of steam injection, to optimize the steam chamber, and to enhance oil recovery [3]. This technology is widely used in Liaohe, Shengli, and Xinjiang oilfields, and the result is that technology can improve reservoir productivity, improve the steam injection uniformity, and enhance the oil recovery [4, 5]. However, there are few theoretical studies on this technology. A steady thermodynamic calculation model of gas-liquid two-phase flow in a steam injection column of multipoint steam injection was established [6], and the vapor injection valve with uniform distribution of the steam injection volume in horizontal wells was optimized as the objective function. However, due to the heterogeneity of the heavy oil reservoir and the effect of the vapor energy loss along the channel after the horizontal well scale implementation, there is a general problem of the heterogeneous production of horizontal tanks in the process of general steam injection [7–9]. Taking into account the above problem, scientists design a distributor that limits multiple flows to horizontal wells, injecting steam into multiple locations of horizontal reservoirs simultaneously through distributors.

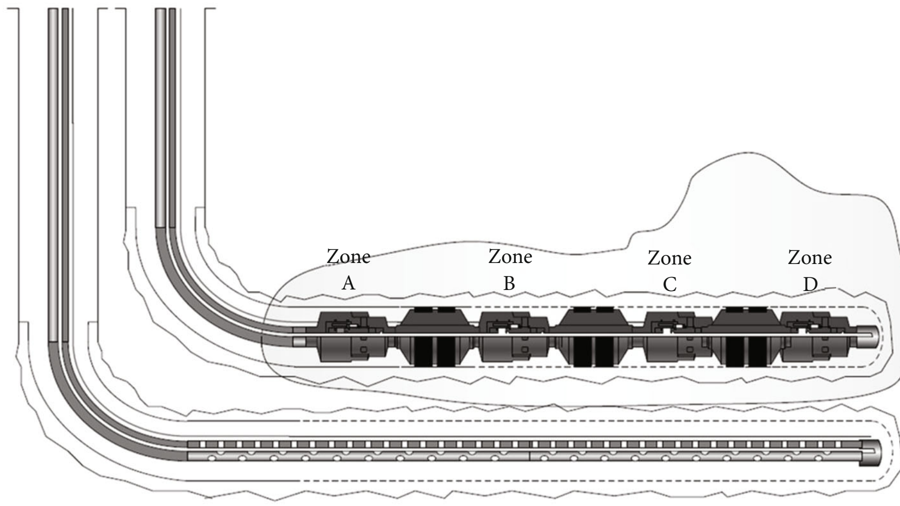

Figure 1: Wellbore structure and steam chamber expansion diagram of multipoint steam injection well.

In previous studies, the uniformity of multipoint steam injection is affected by the steam injection parameters and the location of the steam injection point, and the development of the steam cavity is not uniform, as shown in Figure 1; there are few studies on the optimization of the steam injection device and steam injection parameters [10].

To make stability of superheated steam injected into formation, get the uniform expansion of the steam chamber. First, the mathematical model is presented. Then, three-dimensional numerical simulation was carried out on the multipoint steam injection string, and the variation of parameters along the multipoint steam injection was analyzed to obtain the variable mass flow law of superheated steam in the wellbore. Finally, the steam injection situation under different steam injection volumes and steam injection positions was compared to optimize the steam injection uniformity. However, this paper only optimizes the parameters of steam injection volume and steam injection valve configuration, without considering other potential influencing factors, and will continue to explore and study related influencing factors in the future.

2. Mathematical Model

Fluid flow process in multipoint steam injection horizontal well is shown in Figure 2.

2.1. Basic Assumptions of the Model

(1) The oil reservoir in the horizontal portion is divided equally in the horizontal direction, and the thermal physical parameter of the reservoir does not vary with the change in temperature

(2) When heat is transferred from the well to the outer edge of cementation, steady heat transfer occurs, and unsteady heat transfer occurs when the heat is transferred from the outer edge of the cement ring to the heat storage chamber

(3) The horizontal well is divided into n microsegments, and the vapor injected into the same microsegment is uniformly sucked into the reservoir

2.2. Calculation of Pressure Gradient along the Path. After the saturated vapor is injected into the wellbore, it becomes a gas-liquid two-phase flow, and the gas-liquid two-phase flow is required to calculate the pressure change. According to the pressure gradient equation, the pressure gradient equation mainly includes friction loss pressure gradient, potential energy pressure gradient, and kinetic energy pressure gradient model [11–13].

The pressure gradient equation is expressed as Equation (1) by the conservation of mass and momentum.

$$\frac{\Delta p}{\Delta Z} = \frac{\rho_m g \sin\theta - \tau_f}{1 - \left(i_s q / A_p^2 p\right)}, \tag{1}$$

where p is the pressure at the well point, Pa; Z is the depth, m; ρ_m is wet vapor density, kg/m^3; g is the acceleration of gravity, m/s^2; θ is an angle between the well and the horizontal direction, °; τ_f is the friction loss slope, Pa/m; i_s is the steam mass flow rate, kg/s; q is the volume flow of steam, m^3/s; A_p is the cross-section of the tubing, m^2.

2.3. A Computational Model of Temperature in the Well. The temperature and pressure of saturated steam have a coupling relationship, as shown in the following equation:

$$T_s = 210.2376 p_s^{0.21} - 30, \tag{2}$$

where T_s is the temperature of steam, °C, and P_s is the steam pressure, MPa.

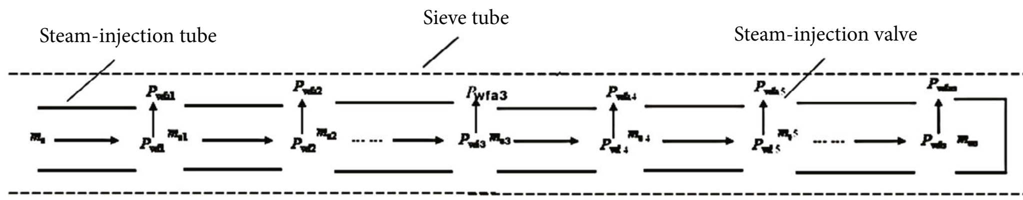

Figure 2: Horizontal well steam injection simulation diagram.

2.4. A Model of Steam Dryness along Well. Based on the law of energy conservation, at the same time and at the same depth, the heat loss is equivalent to the energy loss of the wet steam [14, 15], as shown in the following equation:

$$\frac{dQ}{dZ} = -i_s \frac{\mathrm{dh}_m}{dZ} - i_s \frac{d}{dZ}\left(\frac{v^2}{2}\right) + i_s g, \tag{3}$$

where Q is heat loss, J; h_m is the specific heat enthalpy of wet saturated steam, kJ/kg; v is the wet steam velocity, m/s.

After finishing Equation (3), we can get

$$C_1 \frac{\mathrm{dx}}{dZ} + C_2 x + C_3 = 0. \tag{4}$$

Among them, $C_1 = i_s(h_s - h_w)$.

$$\begin{aligned} C_2 &= i_s\left[\left(\frac{\mathrm{dh}_s}{\mathrm{dp}} - \frac{\mathrm{dh}_w}{\mathrm{dp}}\right)\frac{\mathrm{dp}}{dZ}\right], \\ C_3 &= \frac{dQ}{dZ} + i_s \frac{\mathrm{dh}_s}{\mathrm{dp}}\frac{\mathrm{dp}}{dZ} + \frac{i_s^3}{A^2 \rho}\frac{d}{dZ}\left(\frac{1}{\rho}\right) - i_s g, \end{aligned} \tag{5}$$

where h_s is the specific heat enthalpy of dry saturated steam, kJ/kg, and h_w is a specific enthalpy of saturated water, kJ/kg; drying $x_{z,t}$ of any depth Z is expressed as follows [16]:

$$x_{Z,t} = e^{-(C_2/C_1)Z}\left[-\frac{C_3}{C_2}e^{(C_2/C_1)Z} + x_w + \frac{C_3}{C_2}\right], \tag{6}$$

where x_w is the dryness of the initial injected steam, decimal.

2.5. Friction and Calculation of Work Done by Friction. The calculation is as follows: the microelement segment is subdivided into several smaller microelement segments according to the number of slit rows, and the thermophysical parameters of the fluid on each microelement segment are the same [17, 18]. Firstly, the mass flow rate and flow rate of fluid on each small microelement section are calculated, and then the friction force and frictional work on the microelement segment are calculated [19]. Then, the total friction force and frictional work on the microelement section are calculated by superposition [20–22]. The method provides a more detailed description of fluid flow in a slotted screen horizontal wellbore.

The steam absorption capacity of the reservoir of each row slit is

$$m_{\mathrm{sfl}} = \frac{\mathrm{m_{sf}dl}}{\mathrm{dl}/l_u} = m_{\mathrm{sf}} \cdot l_u. \tag{7}$$

The mass flow of the j row slit is

$$m_{\mathrm{sl}}(j) = m_{\mathrm{s},i} - m_{\mathrm{sfl}} \cdot (j\text{-}1)\left(j = 1, 2, \cdots\cdots, p_{\mathrm{gf}}\right). \tag{8}$$

The average flow velocity on the small and microelement segments is

$$v_{\mathrm{sl}}(j) = \frac{m_{\mathrm{sl}}(j)}{\rho_m A} = \frac{4 m_{\mathrm{sl}}(j)}{\rho_m \pi D_{\mathrm{in}}^2}. \tag{9}$$

In unit time, the work done by the friction force on the microelement segment is expressed as follows [23–25]:

$$\frac{\Delta W(j) = \tau_{\mathrm{cl}}(j) l_u}{l_u / v_{\mathrm{sl}}(j) = \tau_{\mathrm{cl}}(j) v_{\mathrm{sl}}(j)\left(j = 1, 2, \cdots\cdots, p_{\mathrm{gf}}\right)}, \tag{10}$$

where $\tau_{\mathrm{cl}}(j)$ is the friction force between the steam and the inside of the screen tube, N. The calculation method is

$$\tau_{\mathrm{cl}}(j) = f \cdot \rho_{\mathrm{m}} \cdot \frac{\pi D_{\mathrm{in}} l_u}{8} v_{\mathrm{sl}}^2(j)\left(j = 1, 2, \cdots\cdots, p_{\mathrm{gf}}\right). \tag{11}$$

The expression of the work done by the friction force on the segment of length dl in unit time is

$$dW = \sum_{j=1}^{p_{\mathrm{gf}}} \Delta W(j) = \sum_{j=1}^{p_{\mathrm{gf}}} \tau_{\mathrm{cl}}(j) v_{\mathrm{sl}}(j). \tag{12}$$

The expression of friction on the segment dl is [26, 27]

$$\tau_c = \sum_{j=1}^{p_{\mathrm{gf}}} \tau_{\mathrm{cl}}(j) = \sum_{j=1}^{p_{\mathrm{gf}}} f \cdot \rho_m \cdot \frac{\pi D l_u}{8} v_{\mathrm{sl}}^2(j) = \frac{\rho_m \pi D l_u}{8} \sum_{j=1}^{p_{\mathrm{gf}}} f \cdot v_{\mathrm{sl}}^2(j), \tag{13}$$

where f is the dimensionless friction coefficient [28]. The calculation method of friction coefficient between fluid and pipe wall adopts the conventional calculation method of pipe flow [29, 30], and the calculation process is as follows:

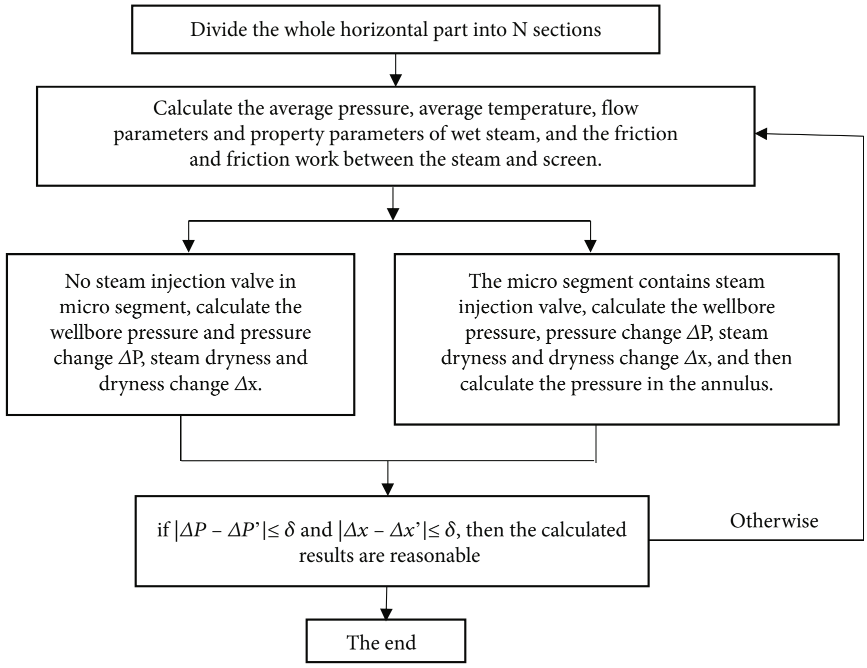

Figure 3: The flow diagram of the calculation model.

(1) Calculate Reynolds number [31–33]

The Reynolds number calculation formula of two-phase flow is as follows:

$$R_e = \frac{v_{\mathrm{sl}}^2(j) \cdot D_{\mathrm{in}} \cdot [\rho_w E_l + \rho_s(1 - E_l)]}{\mu_w E_l + \mu_s(1 - E_l)}, \tag{14}$$

where R_e is Reynolds number; ρ_w and ρ_s are the density of liquid water and dry saturated steam, kg/m^3; μ_w is the viscosity of hot water in water vapor, MPa·s; μ_s is the viscosity of dry saturated steam in water vapor, MPa·s; E_l is the volume liquid content of inlet, dimensionless.

(2) Determine the flow state and calculate the hydraulic friction coefficient [34, 35]

$$\begin{aligned}
&R_e \le 2000,\\
&\quad f = \frac{64}{R_e},\\
&3000 < R_e < \frac{50.9}{\varepsilon^{8/7}},\\
&\quad f = \frac{0.3164}{R_e^{0.25}},\\
&\frac{50.9}{\varepsilon^{8/7}} < R_e < \frac{(665 - 765 \lg \varepsilon)}{\varepsilon},\\
&\quad f = \left\{-1.81 \lg\left[\left(\frac{\varepsilon}{3.7D_{\mathrm{in}}}\right)^{1.11} + \frac{6.9}{R_e}\right]\right\}^{-2}.
\end{aligned} \tag{15}$$

3. Solution of the Model

(1) Vapor pressure, mass flow rate, temperature, and dryness at the heel are known, the whole horizontal part is divided into N sections, and each section is $d_1 = L/N$

(2) The pressure drop change ΔP and dryness change Δx of d_1 length are estimated as the initial values of iterative calculation, and the average pressure, average temperature, flow parameters and property parameters of the wet steam mixture, and the friction and friction work between the steam and the screen are calculated successively

(3) When there is no steam injection valve in the microsegment, the wellbore pressure and pressure change ΔP as well as steam dryness and dryness change Δx in the microsegment are calculated; when the microsegment contains steam injection valve, the wellbore pressure and pressure change ΔP and steam dryness and dryness change Δx in the microsegment are calculated first, and then the pressure in the annulus is calculated

(4) Compare the calculated Δx and ΔP with the estimated Δx and ΔP in step 2; if $|\Delta P - \Delta P'| \le \delta$ and $|\Delta x - \Delta x'| \le \delta$, then the calculated results are reasonable. Otherwise, $\Delta P = \Delta P'$, $\Delta x = \Delta x'$, and return to step 2 to recalculate

(5) Steps 2 to 4 are repeated to calculate the vapor pressure distribution, temperature, and degree of drying on each microsegment until the cumulative length

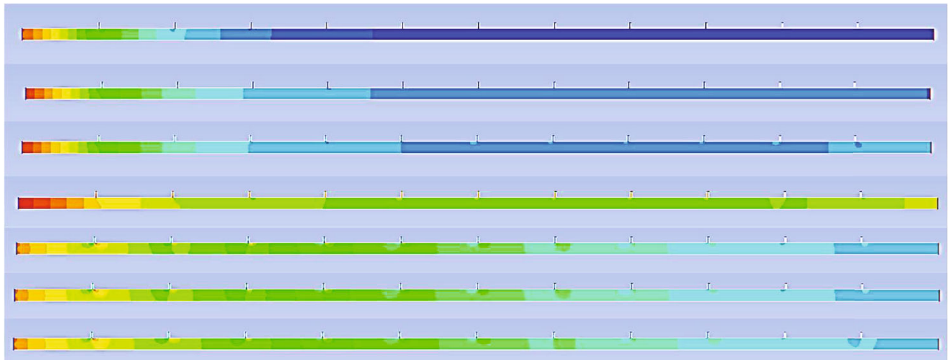

Figure 4: Multipoint steam injection pressure field $t = 3$ s; $t = 6$ s; $t = 9$ s; $t = 12$ s; $t = 15$ s; $t = 18$ s; $t = 21$ s.

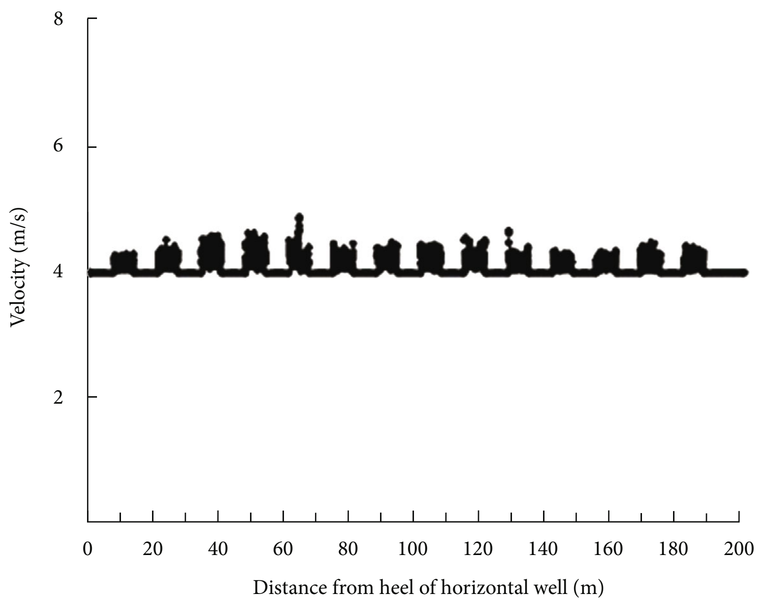

Figure 5: Steam injection velocity distribution curve.

of each microsegment is equal to or greater than the total length of the horizontal well (Figure 3).

4. Case Verification and Analysis

The distribution of pressure field, velocity field, and temperature field in multipoint steam injection wellbore is shown in Figures 4–6. When the steam flows through the steam injection valve, steam flow pressure is reduced, overall speed increased, and temperature decreased, which is close to the changes in the rate of steam injection; the steam valve side first increases then decreases, and the temperature rises after lower first. In order to explore the main factors affecting uniform steam injection, the steam injection velocity, the distance between the steam injection valves, and the steam drying performance are numerically simulated.

Based on the basic geological data of the Maccan River oilfield, a multipoint steam injection horizontal well model was established. The 3-dimensional model data are shown in Tables 1–3.

4.1. Effect of Steam Injection Rate Change on Uniform Steam Injection. In order to explore the influence of the change of steam injection speed on multipoint steam injection, the interval between the opening area of the steam injection valve and the control valve is constant. The quantity of steam injection was performed for 100 m^3/d, 150 m^3/d, and 200 m^3/d (Figure 7); as the amount of steam injection increases, more steam is injected into the reservoir near the horizontal well, resulting in good steam injection uniformity and an increase in cumulative oil production. When the quantity of steam injection reaches 200 m^3/d, the production efficiency is the highest.

4.2. Influence of Changing Steam Injection Valve Spacing on Uniform Steam Injection. The external screen structure remains unchanged, and the steam injection valve spacing was adjusted to 10 m, 20 m, and 30 m, respectively, to reestablish the mathematical model and conduct numerical simulation (Figure 8); with the decrease of steam injection valve spacing, more steam is injected into the reservoir near the heel of the horizontal well, while the steam reaching the

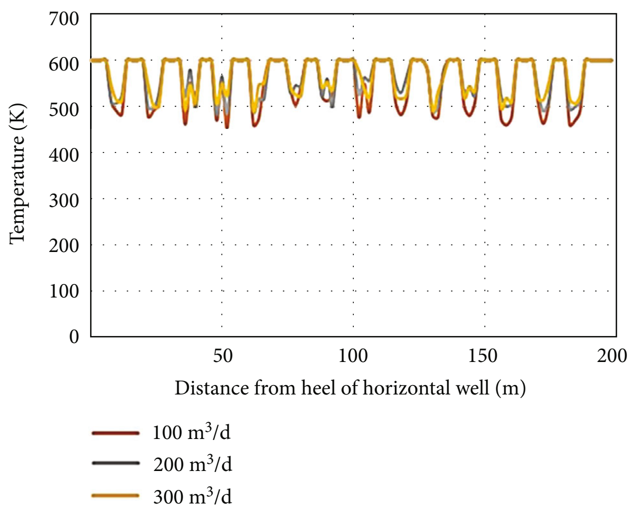

Figure 6: Influence of steam valve distribution on temperature field variation.

Table 1: Heat transfer characteristic data.

Volumetric heat capacity of rock (J/(m^3*C))	0.0000014
Thermal conductivity of rock (m*day*C)	220
Thermal conductivity of water (m*day*C)	0.000002
Thermal conductivity of steam (m*day*C)	2390000

Table 2: Steam injection data.

Horizontal well length (m)	850
Steam injection pressure (MPa)	2
Steam injection rate (kg/s)	1.73
Injection pressure (MPa)	2.12
Steam injection temperature (K)	500
Steam dryness (%)	95

Table 3: Screen structure basic data.

Gap density (slot/m)	446
Gap length (mm)	60
Screen outside diameter (mm)	219.1
Buried depth (m)	450-1400
Sieve tube cut seam wide (mm)	0.3048
Screen inner diameter (mm)	201.2
Slot axial spacing (mm)	7.112
Slot radial spacing (mm)	33.274

toe of the horizontal section gradually decreases; the heating effect of the reservoir near the toe deteriorates, and it brings about the good heating effect of the reservoir near the heel. When the interval of the steam injection valve is 20 m, the ground layer has a good heating effect. The heterogeneity of the steam chamber is more serious if the distance between the steam injection valves is 10 m compared with the steam injection valve. In short, when the number of control valves is 20 m, the injection production profile and the steam

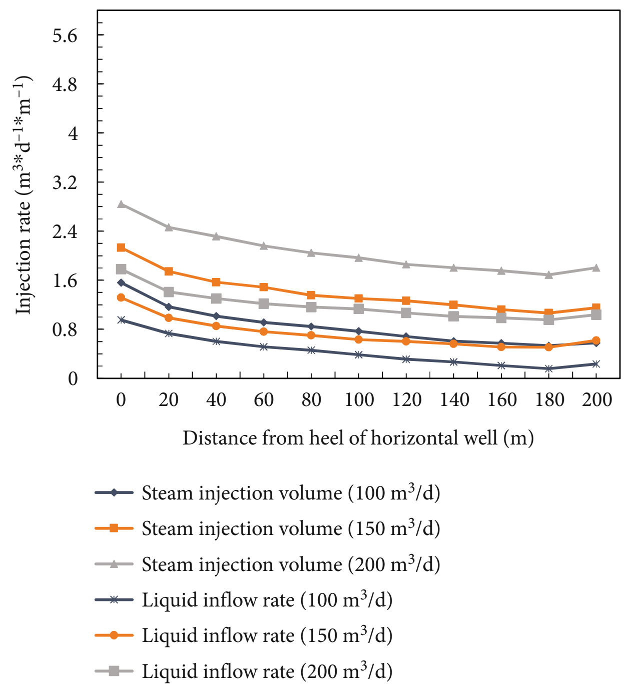

Figure 7: Injection and production profiles with different steam injection volumes.

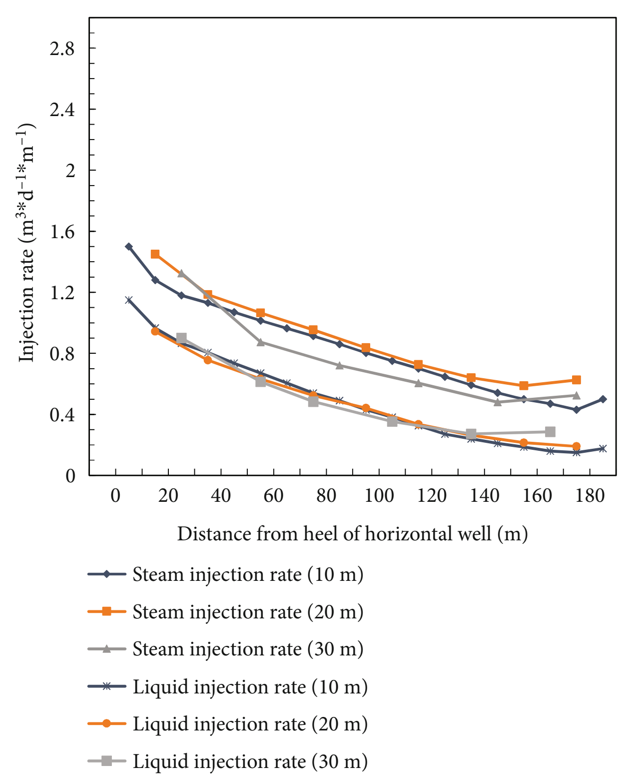

Figure 8: Injection-production profiles with different valve spacing.

chamber are uniformly distributed, and the best steam injection effect can be obtained.

In the schematic diagram of the temperature field change in the wellbore, the steam flow velocity in the steam injection tube is closely related to the position of the steam injection

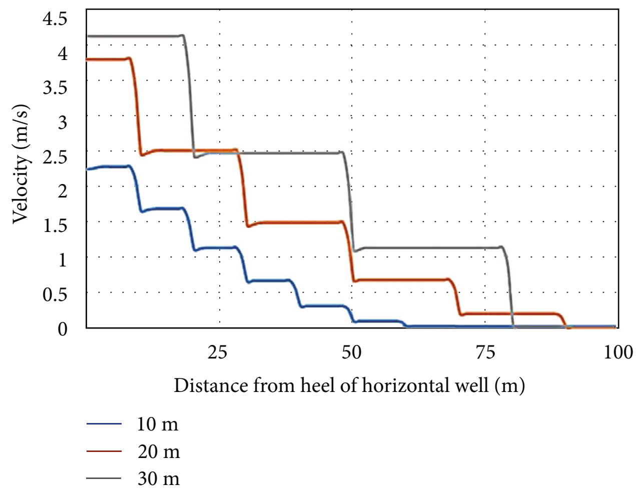

Figure 9: Influence of steam valve distribution on velocity field variation.

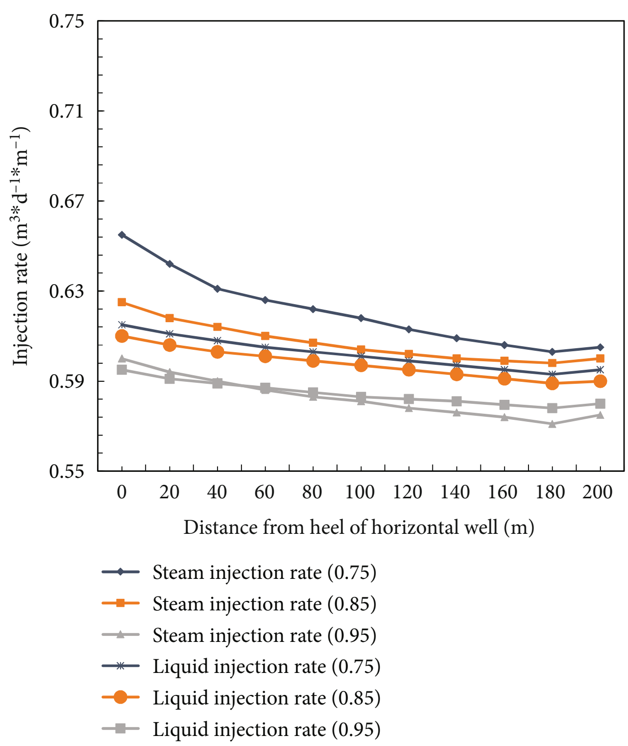

Figure 10: Injection-production profiles with different steam dryness.

valve (Figure 9). Whenever the steam flows into the wellbore annulus through the steam injection valve, the steam speed will drop sharply. In the process of flow in the injection tube, the velocity remains relatively stable.

4.3. Effect of Changing Steam Dryness on Uniform Steam Injection. With the increase in vapor dryness, the vapor density decreases, the steam velocity increases in the well, the friction loss of the vapor in the flow process increases, and the decrease of vapor pressure increases. To explore the influence of steam dryness on the uniformity of steam injection, under the same conditions of other parameters, the variation law of uniform distribution of steam injection profile was compared when the steam dryness was 0.75, 0.85, and 0.95, respectively (Figure 10). With the increase of steam dryness, the average steam inlet flow and liquid inlet flow in the horizontal section of the horizontal well gradually decreased, but the distribution uniformity of the steam injection profile gradually increased.

5. Summary and Conclusions

Characteristics of variable mass flow rate in the steam injection process are considered based on a multipoint steam injection horizontal well. A calculation model of various parameters of multipoint steam injection horizontal well was established. Practical examples of multipoint steam injection are introduced. In order to calculate the vapor parameters along the well in the multipoint steam injection process, the nodal point analysis method is adopted. The effect of the steam injection parameter and the interval of the steam injection valve were analyzed on the vapor parameter along the well in the multipoint steam injection process. The following conclusions can be drawn from this study:

(1) When the steam flows into the steam injection valve, the pressure decreases, the gas-liquid two-phase flow rate accelerates, the temperature decreases remarkably, and the friction loss becomes large

(2) The well injection pressure hardly affects the heat loss of steam injection, and the heat loss in the well decreases with the increase of the distance between steam injection valves. The higher the injection rate, the higher the heat supplement is, the lower the heat loss is, and the higher the dryness of bottomhole steam is

(3) In the actual steam injection process in the mine, the amount of steam injection can be increased appropriately to increase the dry steam at the bottom of the well, and the distance between the steam injection valves cannot be reduced

Data Availability

Data can be obtained from the corresponding author.

Conflicts of Interest

The authors declare that there is no conflict of interest regarding the publication of this paper.

Acknowledgments

This work was supported by the National Science and Technology Major Project (No. 2016ZX05031-002) and the National Natural Science Foundation of China (No. 51704190).

References

[1] F. Sun, Y. Yao, G. Li et al., "An improved two-phase model for saturated steam flow in multi-point injection horizontal wells under steady-state injection condition," *Journal of Petroleum ence & Engineering*, vol. 167, article 0518303620, pp. 844–856, 2018.

[2] P. Li, Y. Zhang, H. Hu, Y. Liu, Y. Liu, and H. Chen, "Optimization of the slotted liners parameters during dual tubing steam injection process," *IOP Conference Series Earth and Environmental Science*, vol. 431, no. 1, article 012042, 2020.

[3] F. Sun, Y. Yao, and X. Li, "The heat and mass transfer characteristics of superheated steam coupled with non-condensing gases in horizontal wells with multi-point injection technique," *Energy*, vol. 143, pp. 995–1005, 2017.

[4] X. Feng, J. Qinghui, Y. Zuyang, and Z. Xiaobo, "Nonlinear flow behavior through rough-walled rock fractures: the effect of contact area," *Computers and Geotechnics*, vol. 102, pp. 179–195, 2018.

[5] H. Chen, M. Li, Q. Di, and C. Liu, "Numerical simulation of the outflow performance for horizontal wells with multiple steam injection valves," *Acta Petrolei Sinica*, vol. 38, no. 6, pp. 696–704, 2017.

[6] S. Huang, M. Cao, Y. Xia, X. Chen, and M. Yang, "Heat and mass transfer characteristics of steam in a horizontal wellbore with multi-point injection technique considering wellbore stock liquid," *International Journal of Heat & Mass Transfer*, vol. 127, pp. 949–958, 2018.

[7] S. F. Xue, H. J. Wang, and G. L. Zhu, "Improved calculation model of suction profile of horizontal well," *Special Oil and Gas Reservoirs*, vol. 15, no. 5, pp. 94–97, 2008.

[8] X. Feng, J. Qinghui, X. Chaoshui, and Z. Xiaobo, "Influences of connectivity and conductivity on nonlinear flow behaviours through three-dimension discrete fracture networks," *Computers and Geotechnics*, vol. 107, pp. 128–141, 2019.

[9] F. Sun, Y. Yao, and G. Li, "Comments on heat and mass transfer characteristics of steam in a horizontal wellbore with multi-point injection technique considering wellbore stock liquid [International Journal of Heat and Mass Transfer 127 (2018) 949-958]," *International Journal of Heat & Mass Transfer*, vol. 132, pp. 1319–1321, 2019.

[10] C. Zhu, X. D. Xu, X. T. Wang et al., "Experimental investigation on nonlinear flow anisotropy behavior in fracture media," *Geofluids*, vol. 2019, Article ID 5874849, 9 pages, 2019.

[11] S. Mozaffari, M. Nikookar, M. R. Ehsani, L. Sahranavard, E. Roayaie, and A. H. Mohammadi, "Numerical modeling of steam injection in heavy oil reservoirs," *Fuel*, vol. 112, pp. 185–192, 2013.

[12] M. R. Chesney, F. Felten, H. S. Hallibuton, and J. Edlebeck, "Design, testing, and field performance of steam-injection flow-control devices for use in SAGD oil recovery," in *SPE Canada heavy oil technical conference*, OnePetro, 2015.

[13] X. P. Liu, Z. S. Zhang, and X. E. Liu, "Simulation model of flow pressure drop coupled with seepage in horizontal wellbore," *Journal of Southwest Petroleum Insitute*, vol. 22, no. 2, pp. 36–39, 2000.

[14] S. Huang, Y. Xia, H. Xiong, H. Liu, and X. Chen, "A three-dimensional approach to model steam chamber expansion and production performance of SAGD process," *International Journal of Heat and Mass Transfer*, vol. 127, no. Part A, pp. 29–38, 2018.

[15] C. Zhu, Y. Lin, and G. Feng, "Influence of temperature on quantification of meso-cracks: implications for physical properties of fine-grained granite," *Lithosphere*, vol. 2021, no. -Special 4, Article ID 7824057, 2021.

[16] C. S. Guo, F. Y. Qu, Y. Liu, J. R. Niu, and Y. Zou, "Simulation of steam injection process for horizontal well with heavy oil recovery," *Heat Transfer Engineering*, vol. 39, no. 13-14, pp. 1283–1295, 2017.

[17] X. F. Ni, S. L. Cheng, C. L. Li, and J. Q. An, "A new model for calculating parameters in steam injection well," *Chinese Journal of Computational Physics*, vol. 22, no. 3, pp. 251–255, 2005.

[18] C. Temizel, C. H. Canbaz, Y. Palabiyik, M. Irani, K. Balaji, and R. Ranjith, "Production optimization through intelligent wells in steam trapping in SAGD operations," in *SPE Western Regional Meeting*, OnePetro, 2019.

[19] Y. Qian, L. Richeng, J. Hongwen, S. Haijian, L. Yu, and L. He, "Experimental study of nonlinear flow behaviors through fractured rock samples after high-temperature exposure," *Rock Mechanics and Rock Engineering*, vol. 52, no. 9, pp. 2963–2983, 2019.

[20] Z. Fan, C. He, and A. Xu, "Calculation model for on-way parameters of horizontal wellbore in the superheated steam injection," *Petroleum Exploration and Development*, vol. 43, no. 5, pp. 798–805, 2016.

[21] M. C. He, Q. Sui, M. Li et al., "Compensation excavation method control for large deformation disaster of mountain soft rock tunnel," *International Journal of Mining Science and Technology*, vol. 32, no. 5, pp. 951–963, 2022.

[22] H. Gu, L. Cheng, S. Huang, B. Bo, Y. Zhou, and Z. Xu, "Thermophysical properties estimation and performance analysis of superheated-steam injection in horizontal wells considering phase change," *Energy Conversion & Management*, vol. 99, pp. 119–131, 2015.

[23] Y. Qian, J. Hongwen, L. Richeng, L. Yu, S. Haijian, and H. Guansheng, "Pore characteristics and nonlinear flow behaviors of granite exposed to high temperature," *Bulletin of Engineering Geology and the Environment*, vol. 79, no. 3, pp. 1239–1257, 2020.

[24] A. Z. Xu, Z. F. Fan, L. He, X. Xue, and B. Bo, "Optimization of superheated steam huff and puff wells sequence in heavy oil reservoir," *Applied Mechanics & Materials*, vol. 295, pp. 3154–3157, 2013.

[25] C. He, A. Xu, Z. Fan et al., "An integrated heat efficiency model for superheated steam injection in heavy oil reservoirs," *Oil & Gas Science and Technology*, vol. 74, no. 2, p. 7, 2019.

[26] P. Li, Y. Zhang, X. Sun, H. Chen, and Y. Liu, "A numerical model for investigating the steam conformance along the dual-string horizontal wells in SAGD operations," *Energies*, vol. 13, no. 15, p. 3981, 2020.

[27] M. Li, H. Chen, Y. Zhang, W. Li, Y. Wang, and M. Yu, "A coupled reservoir/wellbore model to simulate the steam injection performance of horizontal wells," *Energy Technology*, vol. 3, no. 5, pp. 535–542, 2015.

[28] S. F. Kaslusky and K. S. Udell, "A theoretical model of air and steam co-injection to prevent the downward migration of DNAPLs during steam-enhanced extraction," *Journal of Contaminant Hydrology*, vol. 55, no. 3-4, pp. 213–232, 2002.

[29] I. D. Gates and N. Chakrabarty, "Optimization of steam assisted gravity drainage in McMurray reservoir," *Journal of Canadian Petroleum Technology*, vol. 45, no. 9, pp. 54–62, 2006.

[30] L. I. Xiuluan, L. I. Hao, L. U. Jian, J. Hang, and W. Hongzhuang, “3D physical simulation on dual horizontal well SAGD in heterogeneous reservoir,” *Shiyou Xuebao/Acta Petrol Sinica*, vol. 35, no. 3, pp. 536–542, 2014.

[31] Y. Qian, J. Wu, C. Zhu, Q. Wang, and X. Jinyong, “The role of multiple heating and water cooling cycles on physical and mechanical responses of granite rocks,” *Geomechanics and Geophysics for Geo-Energy and Geo-Resources*, vol. 7, no. 3, p. 69, 2021.

[32] M. Desheng, J. Guo, C. Zan, H. Wang, and L. Shi, “Physical simulation of improving the uniformity of steam chamber growth in the steam assisted gravity drainage,” *Petroleum Exploration & Development*, vol. 40, no. 2, pp. 202–207, 2013.

[33] M. Dong, F. Zhang, J. Lv, M. Hu, and Z. Li, “Study on deformation and failure law of soft-hard rock interbedding toppling slope base on similar test,” *Bulletin of Engineering Geology and the Environment*, vol. 79, no. 9, pp. 4625–4637, 2020.

[34] D. Ren, X. Wang, Z. Kou et al., “Feasibility evaluation of CO2 EOR and storage in tight oil reservoirs: a demonstration project in the Ordos Basin,” *Fuel*, vol. 331, article 125652, 2023.

[35] Q. Wang, M. C. He, S. C. Li et al., “Comparative study of model tests on automatically formed roadway and gob-side entry driving in deep coal mines,” *International Journal of Mining Science and Technology*, vol. 31, no. 4, pp. 591–601, 2021.